

Optimized growth of large-size, high quality ZrTe₅ single crystals enabling clear quantum oscillations in electrical transport

Hong Du,^{1,*} Yu Cao,^{1,2,*} Jiahao Chen,³ Tian Liang,⁴ Liang Liu,^{1,2} and Ruidan Zhong^{1,2,†}

¹*Tsung-Dao Lee Institute, Shanghai Jiao Tong University, Shanghai 201210, China*

²*School of Physics and Astronomy, Shanghai Jiao Tong University, Shanghai 200240, China*

³*State Key Laboratory of Low Dimensional Quantum Physics,*

Department of Physics, Tsinghua University, 100084, Beijing, China

⁴*Frontier Science Center for Quantum Information, 100084, Beijing, China*

(Dated: March 16, 2026)

Quantum oscillation with nontrivial Berry phase is one of the characteristics of topological materials. As a Dirac semimetal candidate, zirconium pentatelluride (ZrTe₅) stands out as an intriguing material for investigating topological phase transitions and Dirac fermion physics; however, the extreme sensitivity of its electronic properties to stoichiometric variations and crystalline defects has hindered consistent experimental observation. Here, we report an optimized Te-flux synthesis method designed to produce centimeter-scale, high-quality single crystals meanwhile minimizing extrinsic carrier contamination. Comprehensive morphology, structural and chemical characterization, including scanning electron microscopy, Laue backscattering and Rietveld refinement, confirms a high-purity *Cmcm* phase with excellent crystallinity. Furthermore, magnetotransport measurements reveal a remarkably low Shubnikov-de Haas oscillation onset field ($B \approx 0.38$ T) and access to the quantum limit at $B \approx 1.3$ T, indicative of low carrier density and high carrier mobility. These results demonstrate that growth control is crucial for stabilizing intrinsic electronic behavior in ZrTe₅, establishing a robust platform for exploring topological phase transitions and exotic quantum phenomena in topological semimetals.

I. INTRODUCTION

Quantum oscillations in metallic systems originate from the quantization of the energy states into the Landau levels (LLs), when electrons are subjected to an external magnetic field B and consequently forced into quantized cyclotron motion. As the magnetic field varies, the density of states at the Fermi level is modulated with a periodicity of $1/B$, leading to periodic oscillations in physical quantities. However, for two-dimensional (2D) or three-dimensional (3D) Dirac semimetals (DSMs) featuring topologically robust Dirac nodes with linear dispersion, the Landau quantization is fundamentally different due to the presence of relativistic fermions and nontrivial topology. This leads to exotic phenomena such as large linear magnetoresistance[1, 2], chiral anomaly[3, 4], and anomalous quantum Hall effect[5], all of which are promising for future electronic and spintronic applications. Most strikingly, when all the electrons are condensed into the lowest LL—a regime known as the quantum limit—materials may exhibit new quantum states[6–10]. Reaching this limit requires the magnetic field to be comparable to the quantum oscillation frequency, necessitating either extremely high magnetic field[11] or high-quality samples with low carrier density[12, 13].

ZrTe₅ was initially proposed as a candidate for a quantum spin Hall insulator in the 2D limit, with its bulk phase predicted to manifest as either a strong or weak topological insulator (TI) depending on the interlayer coupling[14]. Despite these predictions, experiments investigations into bulk ZrTe₅ have yielded contradictory conclusions. Some studies reported ZrTe₅ as a weak TI with a global band gap by scanning tunneling microscopy and angle-resolved photoemission spectroscopy[15–18], while others suggested it is a 3D DSM through Shubnikov-de Haas (SdH) quantum oscillation[19–22]. This long-standing discrepancy has been largely reconciled by the consensus that ZrTe₅ sits in close proximity to topological phase boundary between a weak TI and a strong TI regime. At this critical transition point, the formation of a bulk Dirac node allows the system to effectively approximate a DSM state.[23–25]. As a result, the topology property of ZrTe₅ is highly sensitive to sample quality, which can be easily influenced by the growth methods, growth conditions and the measurement environment[26–33]. Systematic studies comparing samples grown via Te-flux and chemical vapor transport indicate that the flux method generally produces crystals closer to ideal stoichiometry with lower carrier density[12, 26]. Nevertheless, a closer inspection of the resistivity anomaly peak temperature (T_p)—which reflects the Fermi level position relative to the Dirac point—reveals that the Fermi surface varies significantly even among flux-grown sam-

* These authors contributed equally to this work.

† rzhong@sjtu.edu.cn

ples. Specifically, flux-grown ZrTe_5 samples in this study[12] exhibit resistivity peaks in the 60–100 K range, while others display a persistent semiconducting behavior extending down to 2 K[26], suggesting a profound sensitivity of the electronic structure to subtle growth variations. Therefore, optimizing the growth of ZrTe_5 to produce controllable, large-size, high-quality crystals is crucial not only for the study of quantum oscillation and reaching quantum limit, but also for comprehensively map the delicate topological properties of ZrTe_5 .

In this paper, we report an optimized Te-flux growth method to synthesize large-size, high-quality ZrTe_5 single crystals with low carrier density. By implementing a strategic thermal oscillation protocol and a crucible-reduced setup, we successfully suppressed the spontaneous nucleation and enlarged the resulting crystal dimensions. Meanwhile, by utilizing purified Te and an alumina filter, we significantly eliminated extrinsic carrier contamination in ZrTe_5 . The superior quality of these crystals is corroborated by comprehensive characterizations via SEM, Laue backscattering, and Rietveld refinement. Most significantly, magnetotransport measurements reveal the onset of SdH oscillations at a remarkably low magnetic field ($B \approx 0.38$ T), with the system entering the quantum limit by $B \approx 1.3$ T. These results not only validate the exceptional sample quality of our crystals, but also provides a robust platform to unravel the topological properties of ZrTe_5 .

II. EXPERIMENTAL DETAILS

A. Optimized sample growth method

Large-scale single crystals of ZrTe_5 were synthesized using an optimized Te-flux method designed to maximize crystal dimensions while minimizing extrinsic carrier density. Given that Te is highly susceptible to oxidation in ambient air, a pre-growth purification was performed, as displayed in Figure 1(a). Raw Te was vacuum-sealed with carbon and annealed at 700°C for 8 hours to reduce oxides and remove volatile impurities. High-purity Zr (99.9999%) and purified Te were utilized in a 1:300 molar ratio. To scale up production and increase crystal size, the starting material mass was increased from 30g to 60g by omitting an internal crucible, allowing the quartz tube itself to act as the primary growth vessel. Furthermore, to prevent contamination from traditional quartz wool, an alumina filter was integrated into the assembly by a pre-necking in the middle of the quartz tube, as illustrated in Figure 1(b). The temperature profile of the growth process is presented in Figure 1(c). The

sealed assembly was heated to 900°C and held for 48 hours to ensure a fully homogenized melt. Following an initial rapid cool-down to 600°C (150 min), the cooling profile was specifically engineered to control nucleation and enhance crystal perfection. The melt was slowly ramped down to 469°C at a rate of $1^\circ\text{C}/\text{h}$ to promote crystallization. This was followed by a swift reheating to 609°C within 10 minutes and then slowly down to 469°C . This rapid remelt process is critical for dissolving smaller and defective nuclei into the flux allowing the solute to recrystallize onto larger, existing single crystals. After several cycles, the furnace was heated to 490°C in 5 minutes. The ampoule was then removed and centrifuged, successfully decanting the molten Te through the alumina filter into the catch crucible and isolating the large-size ZrTe_5 single crystals at the bottom of the tube in Figure 1(d).

B. Measurement methods

The surface morphology and elemental analysis of the prepared single crystal samples were inspected by scanning electron microscopy (SEM) coupled with Energy Dispersive Spectroscopy (EDS) using ZEISS Gemini 300. The crystallinity of the grown crystals was examined by the Laue backscattering technique with a polychromatic source of the x-ray beam. The structural characterization was performed by Powder X-ray diffraction (PXRD), using a Bruker D8 Advance Eco powder diffractometer equipped with (Cu-K_α radiation) ($\lambda = 1.5418$ Å). Rietveld refinement were carried out on the powder diffraction data using the TOPAS v.6.0 software. Electrical connections are made using gold wires and silver paste. Both linear and non-linear electrical transport measurements are conducted using Quantum Design 14T Dynacool. For six-terminal linear transport measurements, longitudinal and transverse resistances are measured using a K6221 AC current source and SR830 lock-in amplifiers. For non-linear transport measurements, signals are monitored by the lock-in technique with harmonic number = 2, relative to the excitation current ($f = 13.777$ Hz).

III. RESULTS AND DISCUSSION

A. Sample Morphology

As shown in Figure 2(a–b), by using the optimized Te-flux method with a thermal oscillation protocol, we successfully scaled the crystal dimensions by nearly an order of magnitude. Initially,

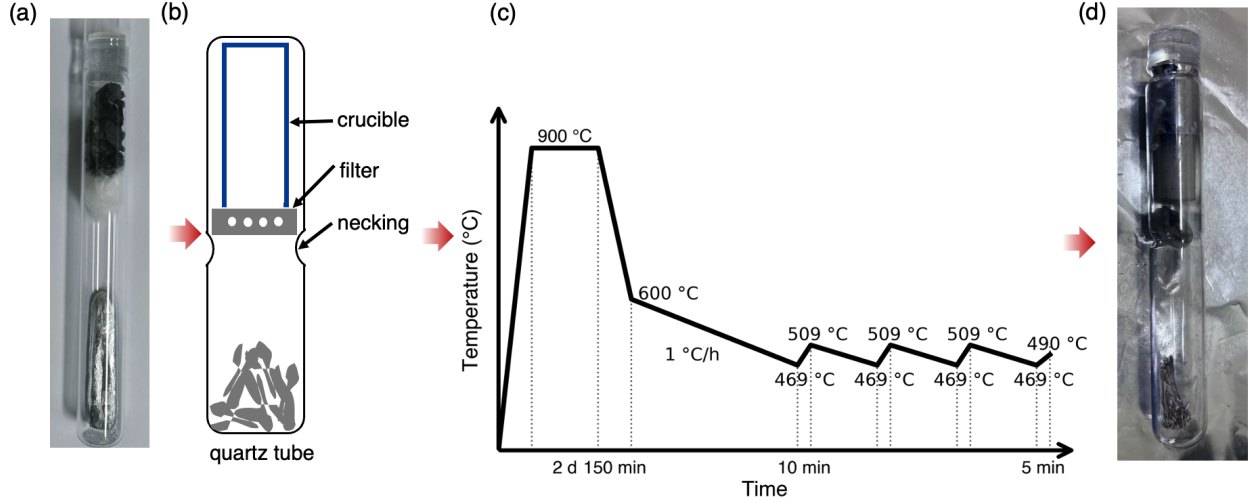


FIG. 1. (a) Purified Te by annealing at 700°C with carbon. (b) Schematic illustration of the growth ampoule assembly, featuring a quartz tube with one catch crucible and a necking design to support a specialized alumina filter. (c) Temperature profile of the optimized Te-flux growth process. (d) Photograph of the quartz tube after centrifugation at 490°C , showing the separation of the residual Te-flux from the harvested ZrTe_5 crystals.

we reproduced typical single crystals measured approximately $2 \times 0.2 \times 0.05 \text{ mm}^3$ following growth protocols described in previous reports[26]. However, by implementing our optimized Te-flux method we consistently attained large-scale crystals reaching up to $10 \times 2 \times 1 \text{ mm}^3$. This substantial enlargement in all three dimensions confirms the effectiveness of the suppressed nucleation approach. The photograph of the as-grown ZrTe_5 crystal exhibit ribbon-like morphology with shiny metallic luster, indicating their high crystallinity and characteristic quasi-two-dimensional structure. Scanning electron microscopy (SEM) characterization shows the resulting crystals have well-defined crystal layers, which corresponds to the the ac plane of crystal structure, while characteristic quasi-1D stripes align with the a -direction.(Figure 2(c)). As shown in the high-magnification micrograph of the crystal corner (Figure 2(d)), the individual layers are clearly stack along the b -axis, which is a direct manifestation of the unique crystal structure of ZrTe_5 . These morphology features, combined with the absence of significant grain boundaries or defects, suggest the high sample quality required to observe clear quantum oscillations in transport measurements.

B. Structural and chemical characterization

ZrTe_5 crystallizes in the orthorhombic layered crystal structure with space group $Cmcm$, as presented in Figure 3(a-b). In the unit cell, one zirconium atom and three tellurium atoms are arranged

into a ZrTe_3 tetrahedron. The ZrTe_3 tetrahedrons run parallel to the a -axis to form infinite quasi-1D chains, which are further linked along the c -axis via zigzag chains of Te atoms to form 2D layers in the ac plane. These two-dimensional ZrTe_5 layers stack along the b -axis via weakly van der Waals forces with a half-period shift between two neighboring layers, forming the 3D bulk crystal. Hence, the single crystals are easy to mechanically exfoliate to thin flakes of ZrTe_5 .

The single crystallinity of ZrTe_5 crystal was examined using the X-ray Laue backscattering measurement. The resulting Laue diffraction pattern, as shown in Figure 3(c), exhibits sharp and clear diffraction spots without any evidence of broadening or splitting, ascertaining the excellent crystal quality. The observed symmetry of the Laue diffraction pattern is in excellent agreement with theoretical calculations for the $Cmcm$ space group along (010) direction, verifying that the large-area facets of the crystal platelets are oriented along the ac plane.

The obtained ZrTe_5 crystals were fully ground to identify the crystal phase by the powder X-ray diffraction (XRD) measurements and Rietveld refinement. As shown in Figure 3(d), all the diffraction peaks can be well fitted and no other phases are detected, confirming the phase purity of the compound. The calculated lattice constants are $a = 3.99 \text{ \AA}$, $b = 14.53 \text{ \AA}$, $c = 13.73 \text{ \AA}$ and the cell volume is 795.1 \AA^3 , which are in close agreement with the previously reported values. The refinements converge well with the reliability factors $R_{wp} = 8.79$, reflecting a reliable fitting result. The detailed information

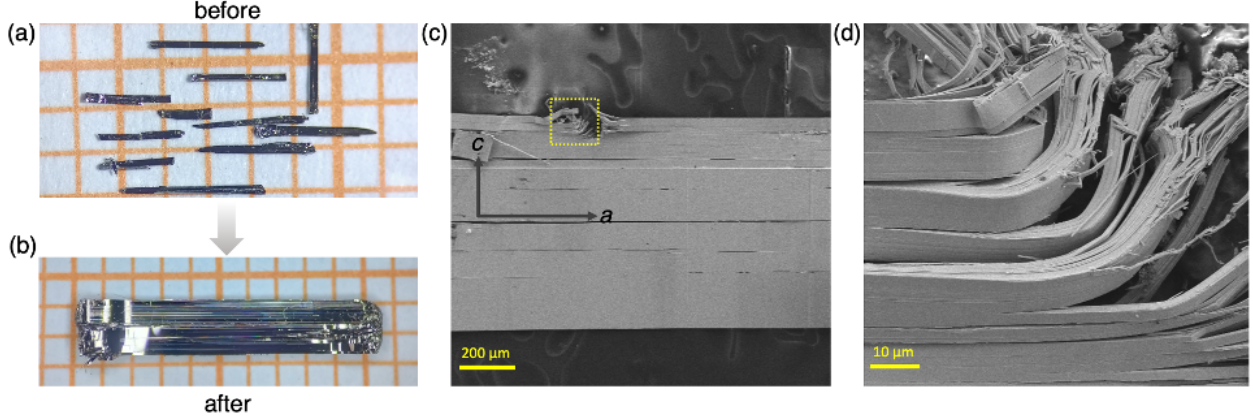


FIG. 2. (a–b) Optical images of typical ZrTe_5 single crystals grown by previously reported method and the optimized Te-flux method, with (b) showing large-size, ribbon-like morphologies with lengths exceeding 1 cm. (c) Scanning electron microscopy (SEM) image of a representative crystal, displaying a flat, high-quality surface. (d) High-magnification SEM image of the area highlighted in (c), revealing the distinct layered structure characteristic of ZrTe_5 .

about the structure refinement is given in Table I. Figure 3(e) shows the XRD results measured on the exposed surface of ZrTe_5 crystals. All the peaks can be indexed to $(0k0)$ planes, indicating that the exposed surface belongs to ac plane. The quality of the crystal was further examined using the X-ray rocking curve, as shown in the inset of Figure 3(e). The X-ray rocking curve of the (020) peak displays a full-width at half-maximum (FWHM) of only 0.06° , confirming the exceptional crystalline mosaicity of the synthesized samples.

Elemental stoichiometry and sample homogeneity were verified by energy-dispersive X-ray spectroscopy (EDS) measurement. The representative spectrum of on numbers of freshly cleaved crystals is shown in Figure 3(f). The average Zr : Te molar ratios are estimated to be 1 : 4.95, which is near to the ideal stoichiometric ratio. The element mappings of Zr and Te, presented in Figure 3(g), shows the uniform distribution of Zr and Te, strongly suggesting that the growth is homogeneous in the synthesized samples. The above comprehensive structural characterizations, together with the elemental analysis rigorously demonstrates the high single-crystalline quality and phase purity achieved through the optimized Te-flux growth method.

C. Transport measurement

To verify the sample quality through electrical transport, the longitudinal resistivity (ρ_{xx}) and Hall resistivity (ρ_{xy}) were measured at 1.9 K. As illustrated in Figure 4(a), the zero-field resistivity exhibits a characteristic increase upon cooling, peaking

at a temperature $T_p = 90$ K. This peak is attributed to a temperature-induced Lifshitz transition, where the Fermi level shifts across the Dirac point, leading to a crossover in the dominant carrier species. The high quality of the optimized crystals is most prominently evidenced by the observation of pronounced Shubnikov-de Haas (SdH) quantum oscillations. Figure 4(b) shows the longitudinal resistivity (ρ_{xx}) as the functions of the perpendicular magnetic field (B , applied along the b -axis). Oscillations in ρ_{xx} can be well observed and start at a low onset field of $B_{int} \approx 0.38$ T, which indicates the extremely high mobility in our flux-grown crystals. Hall mobility and carrier concentrations are obtained by low-magnetic-field Hall measurements (Fig. 4(c)), from which we extract the density $n = 9.20 \times 10^{16} \text{ cm}^{-3}$ and mobility $\mu = 5.58 \times 10^5 \text{ cm}^2\text{V}^{-1}\text{s}^{-1}$. Notably, a kink is observed in the magnetoresistance near $B \approx 1.3\text{T}$, signifying the system's entry into the quantum limit. This feature persists when the magnetic field is tilted from the out-of-plane direction (b -axis) toward the in-plane direction (c -axis), suggesting the robustness of the quantum limit in this 3D Dirac semimetal.

IV. CONCLUSION

In conclusion, we have developed an optimized Te-flux synthesis technique that effectively suppresses the spontaneous nucleation and eliminates extrinsic carrier contamination in ZrTe_5 . The strategic use of purified precursor, specialized growth assembly and a thermal oscillation profile enabled the growth of centimeter-scale single crystals with exceptional

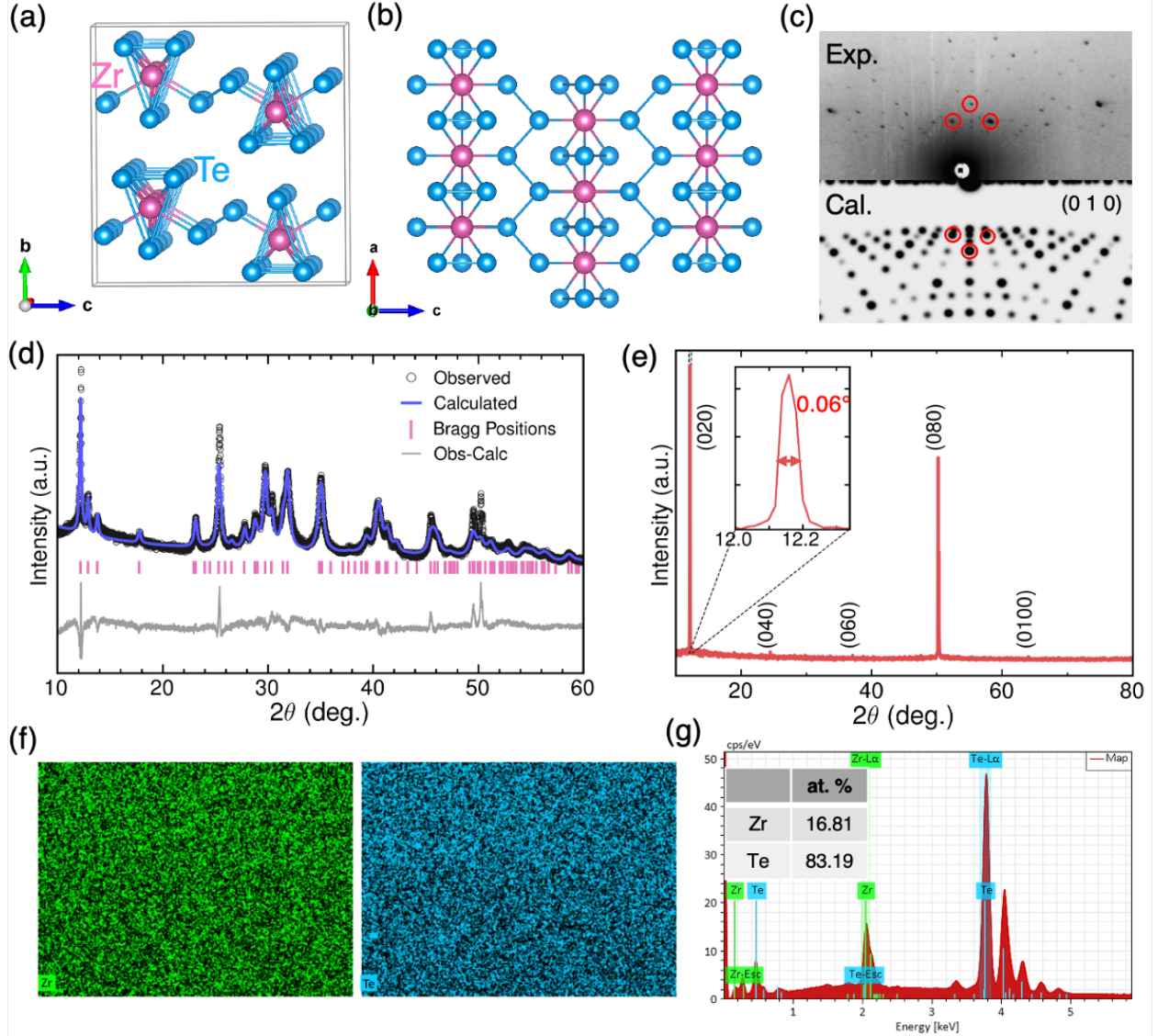


FIG. 3. (a–b) Schematic illustration of the orthorhombic crystal structure of ZrTe_5 viewed along the a - and b -axes, highlighting the 1D ZrTe_3 chains and the layered 2D structure. (c) Laue backscattering pattern of a flux-grown single crystal, showing sharp, well-defined spots that match the calculated pattern (bottom). (d) Powder X-ray diffraction (XRD) pattern and Rietveld refinement of crushed ZrTe_5 crystals. (e) XRD pattern of a ZrTe_5 single crystal showing $(0k0)$ reflections. Insets show a rocking curve of the (020) peak with a FWHM of 0.06° . (f) EDS elemental mapping for Zr (green) and Te (blue), showing a uniform distribution of elements across the crystal. (g) EDS spectrum confirming the chemical composition, with an atomic ratio of approximately 1:4.95, indicating near-ideal stoichiometry.

structural perfection. Comprehensive characterization via SEM, Laue backscattering, and Rietveld refinement confirms the synthesis of a high-purity $Cmcm$ phase. The high crystalline quality is further validated by the emergence of Shubnikov-de Haas oscillations at a remarkably low onset field of 0.38 T. Furthermore, the observation of a distinct Hall resistivity signature at $B \approx 1.3$ T signifies the system's entry into the quantum limit, substantiating the efficacy of this growth optimization. This work

provides a controllable methodology for harvesting high-quality ZrTe_5 , establishing a robust platform for further exploring the sensitive topological phase transitions and exotic quantum phenomena inherent to this Dirac semimetal candidate.

TABLE I. Crystallographic data and structure refinement of ZrTe₅ single crystals at room temperature.

Refined Formula	ZrTe ₅	Atom	Wyckoff	x	y	z	Occ.
Crystal system	Orthorhombic	Te(1)	8 <i>f</i>	0.0000	0.07010	0.14940	1
Space group	<i>Cmcm</i> (No. 63)	Te(2)	8 <i>f</i>	0.0000	0.20990	0.56470	1
a (Å)	3.9866(4)	Te(3)	4 <i>e</i>	0.0000	0.33650	0.25000	1
b (Å)	14.5276(1)	Zr	4 <i>e</i>	0.0000	0.68570	0.25000	1
c (Å)	13.7286(9)						
V (Å ³)	795.11(2)						
Density (g/cm ³)	6.092	θ range (deg)	R_{exp} (%)	R_{wp} (%)	R_p (%)	GOF	
Formula weight	729.22	5–30	3.83	8.79	6.74	2.30	

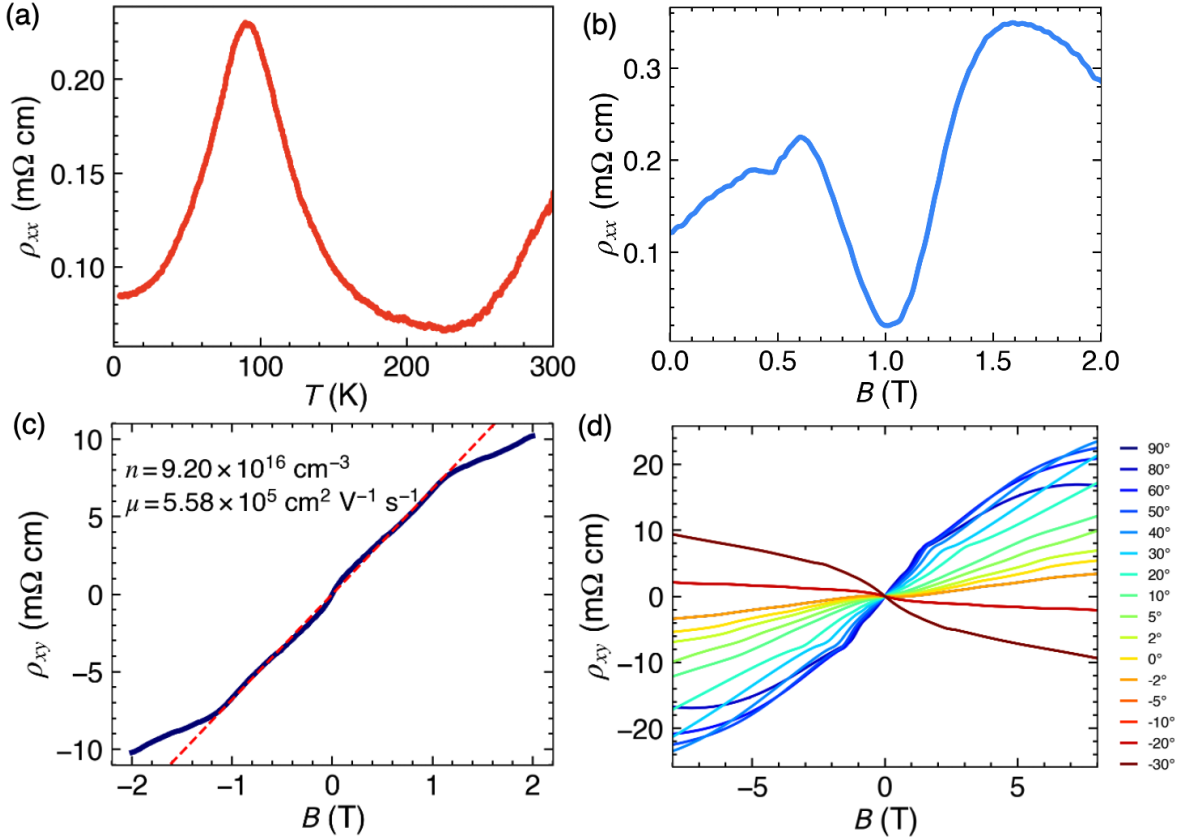


FIG. 4. (a) Temperature dependence of the longitudinal resistivity ρ_{xx} , showing the characteristic resistivity anomaly peak at $T_p \approx 90$ K. (b) Low-temperature ρ_{xx} versus magnetic field $\mu_0 H$, exhibiting clear Shubnikov-de Haas (SdH) oscillations at remarkably low onset fields ($B \approx 0.38$ T), confirming high mobility. (c) Hall resistivity ρ_{xy} at $T = 1.9$ K. The dashed line represents a linear fit for $|B| < 0.6$ T, from which an ultra-low carrier density ($n = 9.20 \times 10^{16} \text{ cm}^{-3}$) and ultra-high mobility ($\mu = 5.58 \times 10^5 \text{ cm}^2 \text{ V}^{-1} \text{ s}^{-1}$) are extracted. (d) Angle-dependent ρ_{xy} curves as the magnetic field is rotated from the b -axis to the ac plane.

ACKNOWLEDGMENTS

The work was supported by the National Key R&D of China under 2021YFA1401600 and 2022YFA1402702, National Natural Science Foun-

dation of China with Grants Nos. 12334008, and 12374148. The experimental support from the Instrumental Analysis Center at Shanghai Jiao Tong University, especially in performing the EDS analyses.

-
- [1] T. Liang, Q. Gibson, M. N. Ali, M. Liu, R. J. Cava, and N. P. Ong, Ultrahigh mobility and giant magnetoresistance in the Dirac semimetal Cd₃As₂, *Nature Materials* **14**, 280 (2015).
- [2] C. Shekhar, A. K. Nayak, Y. Sun, M. Schmidt, M. Nicklas, I. Leermakers, U. Zeitler, Y. Skourski, J. Wosnitza, Z. Liu, Y. Chen, W. Schnelle, H. Borrmann, Y. Grin, C. Felser, and B. Yan, Extremely large magnetoresistance and ultrahigh mobility in the topological Weyl semimetal candidate NbP, *Nature Physics* **11**, 645 (2015).
- [3] S. A. Parameswaran, T. Grover, D. A. Abanin, D. A. Pesin, and A. Vishwanath, Probing the Chiral Anomaly with Nonlocal Transport in Three-Dimensional Topological Semimetals, *Physical Review X* **4**, 031035 (2014).
- [4] E. V. Gorbar, V. A. Miransky, and I. A. Shovkovy, Chiral anomaly, dimensional reduction, and magnetoresistivity of Weyl and Dirac semimetals, *Physical Review B* **89**, 085126 (2014).
- [5] S. Nishihaya, H. Ishizuka, Y. Deguchi, A. Nakamura, T. Yoneda, H. Lee, M. Kriener, and M. Uchida, Anomalous Hall Effect in the Dirac Semimetal Cd₃As₂ Probed by In-Plane Magnetic Field, *Physical Review Letters* **135**, 106603 (2025).
- [6] Z. Song, Z. Fang, and X. Dai, Instability of Dirac semimetal phase under a strong magnetic field, *Physical Review B* **96**, 235104 (2017).
- [7] N. P. Armitage, E. J. Mele, and A. Vishwanath, Weyl and Dirac semimetals in three-dimensional solids, *Reviews of Modern Physics* **90**, 015001 (2018).
- [8] Z. Pan and R. Shindou, Ground-state atlas of a three-dimensional semimetal in the quantum limit, *Physical Review B* **100**, 165124 (2019).
- [9] Z. Sun, Z. Xiang, Z. Wang, J. Zhang, L. Ma, N. Wang, C. Shang, F. Meng, L. Zou, Y. Zhang, and X. Chen, Magnetic field-induced electronic phase transition in the Dirac semimetal state of black phosphorus under pressure, *Science Bulletin* **63**, 1539 (2018).
- [10] W. Sun, Z. Wan, Q. Qian, and G. Qiu, Recent progress on quantum Hall effect in unconventional material systems, *Applied Physics Letters* **126**, 020501 (2025).
- [11] Y. Zhao, H. Liu, C. Zhang, H. Wang, J. Wang, Z. Lin, Y. Xing, H. Lu, J. Liu, Y. Wang, S. M. Brombosz, Z. Xiao, S. Jia, X. C. Xie, and J. Wang, Anisotropic Fermi Surface and Quantum Limit Transport in High Mobility Three-Dimensional Dirac Semimetal Cd₃As₂, *Physical Review X* **10.1103/PhysRevX.5.031037** (2015).
- [12] F. Tang, Y. Ren, P. Wang, R. Zhong, J. Schneeloch, S. A. Yang, K. Yang, P. A. Lee, G. Gu, Z. Qiao, and L. Zhang, Three-dimensional quantum Hall effect and metal-insulator transition in ZrTe₅, *Nature* **569**, 537 (2019).
- [13] D. Xing, B. Tong, S. Pan, Z. Wang, J. Luo, J. Zhang, and C.-L. Zhang, Rashba-splitting-induced topological flat band detected by anomalous resistance oscillations beyond the quantum limit in ZrTe₅, *Nature Communications* **15**, 4407 (2024).
- [14] H. Weng, X. Dai, and Z. Fang, Transition-Metal Pentatelluride ZrTe₅ and HfTe₅ : A Paradigm for Large-Gap Quantum Spin Hall Insulators, *Physical Review X* **4**, 011002 (2014).
- [15] R. Wu, J.-Z. Ma, S.-M. Nie, L.-X. Zhao, X. Huang, J.-X. Yin, B.-B. Fu, P. Richard, G.-F. Chen, Z. Fang, X. Dai, H.-M. Weng, T. Qian, H. Ding, and S. H. Pan, Evidence for Topological Edge States in a Large Energy Gap near the Step Edges on the Surface of ZrTe₅, *Physical Review X* **6**, 021017 (2016).
- [16] Z. Fan, Q.-F. Liang, Y. B. Chen, S.-H. Yao, and J. Zhou, Transition between strong and weak topological insulator in ZrTe₅ and HfTe₅, *Scientific Reports* **7**, 45667 (2017).
- [17] H. Xiong, J. A. Sobota, S.-L. Yang, H. Soifer, A. Gauthier, M.-H. Lu, Y.-Y. Lv, S.-H. Yao, D. Lu, M. Hashimoto, P. S. Kirchmann, Y.-F. Chen, and Z.-X. Shen, Three-dimensional nature of the band structure of ZrTe₅ measured by high-momentum-resolution photoemission spectroscopy, *Physical Review B* **95**, 195119 (2017).
- [18] Y. Zhang, C. Wang, L. Yu, G. Liu, A. Liang, J. Huang, S. Nie, X. Sun, Y. Zhang, B. Shen, J. Liu, H. Weng, L. Zhao, G. Chen, X. Jia, C. Hu, Y. Ding, W. Zhao, Q. Gao, C. Li, S. He, L. Zhao, F. Zhang, S. Zhang, F. Yang, Z. Wang, Q. Peng, X. Dai, Z. Fang, Z. Xu, C. Chen, and X. J. Zhou, Electronic evidence of temperature-induced Lifshitz transition and topological nature in ZrTe₅, *Nature Communications* **8**, 15512 (2017).
- [19] G. Zheng, J. Lu, X. Zhu, W. Ning, Y. Han, H. Zhang, J. Zhang, C. Xi, J. Yang, H. Du, K. Yang, Y. Zhang, and M. Tian, Transport evidence for the three-dimensional Dirac semimetal phase in ZrTe₅, *Physical Review B* **10.1103/PhysRevB.93.115414** (2016).
- [20] W. Yu, Y. Jiang, J. Yang, Z. L. Dun, H. D. Zhou, Z. Jiang, P. Lu, and W. Pan, Quantum Oscillations at Integer and Fractional Landau Level Indices in Single-Crystalline ZrTe₅, *Scientific Reports* **6**, 35357 (2016).
- [21] J. Wang, J. Niu, B. Yan, X. Li, R. Bi, Y. Yao, D. Yu, and X. Wu, Vanishing quantum oscillations in Dirac semimetal ZrTe₅, *Proceedings of the National Academy of Sciences* **115**, 9145 (2018).
- [22] W. Wang, X. Zhang, H. Xu, Y. Zhao, W. Zou, L. He, and Y. Xu, Evidence for Layered Quantized Transport in Dirac Semimetal ZrTe₅, *Scientific Reports* **8**, 5125 (2018).
- [23] J. Hu and S.-Y. Xu, Transport of Topological Semimetals, *Annual Review of Materials Research* (2019).
- [24] Z. Tajkov, D. Nagy, K. Kandrai, J. Koltai, L. Oroszlány, P. Süle, Z. E. Horváth, P. Vancsós, L. Tapasztó, and P. Nemes-Incze, Revealing the topological phase diagram of ZrTe₅ using the com-

- plex strain fields of microbubbles, *npj Computational Materials* **8**, 177 (2022).
- [25] C. Chen Ye, Y. Kreminska, J. Ye, and J. Sławińska, First-principles studies of fermiology in topological phases of bulk ZrTe₅, *Physical Review Materials* **9**, 054204 (2025).
- [26] P. Shahi, D. J. Singh, J. P. Sun, L. X. Zhao, G. F. Chen, Y. Y. Lv, J. Li, J.-Q. Yan, D. G. Mandrus, and J.-G. Cheng, Bipolar Conduction as the Possible Origin of the Electronic Transition in Pentatellurides: Metallic vs Semiconducting Behavior, *Physical Review X* **8**, 021055 (2018).
- [27] S.-S. Chen, X. Li, Y.-Y. Lv, L. Cao, D. Lin, S.-H. Yao, J. Zhou, and Y. Chen, Electrical, magnetotransport and significant thermoelectric properties of Te-rich ZrTe_{5+δ} polycrystals, *Journal of Alloys and Compounds* **764**, 540 (2018).
- [28] J. Mutch, W.-C. Chen, P. Went, T. Qian, I. Z. Wilson, A. Andreev, C.-C. Chen, and J.-H. Chu, Evidence for a strain-tuned topological phase transition in ZrTe₅, *Science Advances* **5**, eaav9771 (2019).
- [29] P. Zhang, R. Noguchi, K. Kuroda, C. Lin, K. Kawaguchi, K. Yaji, A. Harasawa, M. Lippmaa, S. Nie, H. Weng, V. Kandyba, A. Giampietri, A. Barinov, Q. Li, G. D. Gu, S. Shin, and T. Kondo, Observation and control of the weak topological insulator state in ZrTe₅, *Nature Communications* **12**, 406 (2021).
- [30] S. Galeski, T. Ehmcke, R. Wawrzyńczak, P. M. Lozano, K. Cho, A. Sharma, S. Das, F. Küster, P. Sessi, M. Brando, R. KÜchler, A. Markou, M. König, P. Swekis, C. Felser, Y. Sassa, Q. Li, G. Gu, M. V. Zimmermann, O. Ivashko, D. I. Gorbunov, S. Zherlitsyn, T. Förster, S. S. P. Parkin, J. Wosnitza, T. Meng, and J. Gooth, Origin of the quasi-quantized Hall effect in ZrTe₅, *Nature Communications* **12**, 3197 (2021).
- [31] A. Gaikwad, S. Sun, P. Wang, L. Zhang, J. Cano, X. Dai, and X. Du, Strain-tuned topological phase transition and unconventional Zeeman effect in ZrTe₅ microcrystals, *Communications Materials* **3**, 94 (2022).
- [32] W. Song, L. Zhao, X. Wu, Z. Wang, Q. Liu, M. Li, H. Ma, P. Ding, G.-D. Gu, G.-F. Chen, and S.-C. Wang, Temperature dependence of band shifts induced by impurity ionization in ZrTe₅, *Physical Review B* **106**, 115124 (2022).
- [33] Y. A. Salawu, D. Adhikari, J. H. Kim, J.-S. Rhyee, M. Sasaki, K.-S. Kim, and H.-J. Kim, Nonlinear electrical transport phenomena as fingerprints of a topological phase transition in ZrTe₅, *Communications Materials* **4**, 111 (2023).